The Astrophysical Journal Letters, 869:L36 (7pp), 2018 December 20 https://doi.org/10.3847/2041-8213/aaf73e

Chandra Detection of the Circumnuclear Molecular Torus of the Compton-thick Active Galactic Nucleus in NGC 5643

G. Fabbiano[1], A. Paggi[2,3,4], A. Siemiginowska[1], and M. Elvis[1]
[1] Harvard–Smithsonian Center for Astrophysics, 60 Garden Street, Cambridge, MA 02138, USA
[2] Dipartimento di Fisica, Universita' degli Studi di Torino, via Pietro Giuria 1, I-10125 Torino, Italy
[3] Istituto Nazionale di Fisica Nucleare, Sezione di Torino, via Pietro Giuria 1, I-10125 Torino, Italy
[4] INAF-Osservatorio Astrofisico di Torino, via Osservatorio 20, I-10025 Pino Torinese, Italy
Received 2018 November 19; accepted 2018 December 6; published 2018 December 20

Abstract

We report a clumpy elongated feature found with deep *Chandra* Advanced CCD Imaging Spectrometer high-resolution imaging of the Fe Kα line emission in the nuclear region of the Compton-thick active galactic nucleus galaxy NGC 5643. This feature extends for ~65 pc north to south (N-S). No corresponding feature is seen in the 3.0–6.0 keV continuum. The Fe Kα feature is spatially consistent with the N-S elongation found in the CO(2–1) high-resolution imaging with the Atacama Large Millimeter/submillimeter Array, but slightly more extended than the rotating molecular disk of diameter 26 pc indicated by the kinematics of the CO(2–1) line. The *Chandra* detection of a corresponding north to south structure in the neutral Fe Kα line would argue for both CO and Fe Kα emission originating from the obscuring torus.

Key words: galaxies: individual (NGC 5643) – galaxies: Seyfert – X-rays: galaxies

1. Introduction

NGC 5643 is a face-on barred southern galaxy (J2000 R.A. = $14^h32^m40\overset{s}{.}743$, decl. = $-44^d10^m27\overset{s}{.}86$) hosting a Compton-thick active galactic nucleus (CT AGN) with nuclear $N_H > 10^{24}$ cm^{-2} (Risaliti et al. 1999). This AGN has a double-sided ionization cone in the direction of a double radio jet originating from the nucleus (Morris et al. 1985; Schmitt et al. 1994; Cresci et al. 2015). NGC 5643 has been observed with several X-ray observatories to both study its active nucleus, and more recently, its population of galactic sources including an ultra-luminous X-ray source (e.g., Guainazzi et al. 2004; Matt et al. 2013; Annuar et al. 2015). Recent Atacama Large Millimeter/submillimeter Array (ALMA) observations (Alonso-Herrero et al. 2018) have led to the discovery of a nuclear rotating obscuring disk with a 26 pc diameter in this AGN ($0\overset{''}{.}3$, given the assumed distance of 16.9 Mpc; for ease of comparison, we assume the same distance in this Letter). This molecular disk is oriented in the north–south (N-S) direction, perpendicular to the ionization cone. This disk could be related to the obscuring torus of the standard AGN model, responsible for the nuclear obscuration and for the collimation of the ionization cone.

There have been reports with *Chandra* imaging of features possibly connected with the obscuring torus in AGNs, but never in conjunction with an independent observational validation of the existence of this torus. Extended clumpy emission in the 3–6 keV continuum and in the Fe Kα line emission (both neutral and ionized) have been discovered in the nearby CT AGN NGC 4945 with *Chandra* (Marinucci et al. 2012, 2017) and related to the obscuring torus. More recently, we have discovered clumpy Fe Kα emission within ~30 pc of the nucleus of the CT AGN ESO 428-G014, and suggested that this emission originates from the fluorescent emission of the nuclear photons interacting with thick obscuring clouds (Fabbiano et al. 2018c). The detection of the circumnuclear disk in CO(2–1) emission with ALMA in NGC 5643, and the existence of a deep *Chandra* ACIS data set for this galaxy, provide a unique opportunity for exploring both millimeter and X-ray diagnostics of a molecular optical disk torus in CT AGNs.

The only report available in the literature of the morphology of the hard continuum and Fe Kα nuclear emission in NGC 5643 is consistent with a *Chandra* point source (Annuar et al. 2015). However, the *Chandra* data used by Annuar et al. (2015; ObsID 5636) were the result of a very short (7.6 ks), $4'$ off-axis ACIS observation, where the point-spread function (PSF) would be significantly wider (90% encircled energy fraction $>3''$; Chandra Proposers' Observatory Guide (POG): http://cxc.harvard.edu/proposer/POG/html/chap4.html). Subsequently, NGC 5643 has been observed twice with ACIS, with the AGN at the aim point of the *Chandra* telescope, resulting on a total exposure of 113.4 ks. In this Letter, we report the results of the analysis of this deep *Chandra* data set, where the nucleus is observed at the best possible angular resolution. This analysis led to the discovery of the N-S extended emission of the nuclear Fe Kα emission of NGC 5643.

2. Data and Analysis

Table 1 summarizes the two observations of NGC 5643 used for this study. These are the only two observations in the *Chandra* archive that place the nucleus of NGC 5643 at the aim point, resulting in the best possible angular resolution. The data and basic reduction and analysis procedures used here closely follow those used in our previous work (e.g., Fabbiano et al. 2018b, 2018c where we report the spatial analysis of the nucleus of the CT AGN ESO 428-G014).

All of the data sets were screened for high background times, processed to enable a subpixel analysis, and merged using standard Chandra Interactive Analysis of Observations (CIAO; see Fruscione et al. 2006) tools (http://cxc.cfa.harvard.edu/ciao/).

We use a 1/8 subpixel binning for this analysis (the ACIS instrument pixel is $0\overset{''}{.}492$; see Fabbiano et al. 2018b, 2018c for discussions on and similar applications of subpixel binning).

Table 1
Observation Log

ObsID	Instrument	T_{exp}(ks)	PI	Date
17031	ACIS-S	71.9	Fabbiano	2015 May 21
17664	ACIS-S	41.5	Fabbiano	2015 Dec 26

For our analysis, we used CIAO 4.8 tools and the display application DS9 (http://ds9.si.edu/site/Home.html), which is also packaged with CIAO. To highlight some of the features, we applied a Gaussian kernel smoothing to the images, as described in the figure captions.

The *Chandra* PSF was simulated using rays produced by the Chandra Ray Tracer (http://cxc.harvard.edu/ciao/PSFs/chart2/) projected on the image plane by *MARX* (http://space.mit.edu/CXC/MARX/). We refer to Fabbiano et al. (2018c) for an in-depth discussion and validation of the shape of the *Chandra* PSF at the energies considered in this Letter and using subpixel data.

We checked each individual file to ensure that the N-S extended 6.2–6.6 keV feature that we are reporting in this Letter is not a by-product of the PSF anomaly (http://cxc.harvard.edu/ciao/caveats/psf_artifact.html). Both the orientation of the N-S feature and the relative intensity of the extended versus central emission exclude this possibility. The artifact is expected to show a southeast (S-E) direction in ObsID 17664 and a southwest (S-W) direction in ObsID 17031, contrary to the N-S extension in the data. Moreover, the artifact may display ∼6% of the source counts, much less than detected in the N-S extension (see below, Figure 3).

We merged the two observations in Table 1, using the several bright point sources detected in the ACIS field to cross-match the images, excluding the central source of NGC 5643. All of these sources were consistent with being point-like after merging. The images from each ObsID and the merged image all show clear evidence of extended emission from the ionization cone and a bright nuclear source. These features have different spectral signatures (as in the case of other CT AGNs, see Levenson et al. 2006; Fabbiano et al. 2018a). Figure 1 shows the spectral count distribution of all of the data connected with the extended and nuclear emission of NGC 5643 (no detected point sources are in the extraction area, so this is the *Chandra* spectrum of CT AGN emission). This spectrum shows soft emission-line dominated emission at energies below 2.5 keV, which is connected with the extended ionization cone (and will be discussed elsewhere). At higher energies, the spectrum is dominated by a featureless flat continuum and by the Fe Kα neutral emission line at 6.4 keV. As in our study of ESO 428-G014, we imaged hard continuum (3.0–6.0 keV) and Fe Kα emission (6.2–6.6 keV) separately. These images are shown in Figures 2 and 3, compared with the PSF appropriate for these energies and focal plane position. Figure 2 shows that the 3.0–6.2 keV continuum source is somewhat extended (this will be discussed elsewhere), but with no pronounced directionality of the surface brightness. Instead the 6.2–6.6 keV image shows a marked N-S extension in the nuclear source (bottom right panel). This extent is also present in the same band, and with the same directionality, in each of the two separate observations (Figure 3, left panels). This and the point-like appearance of the continuum emission peak exclude bad astrometry in the merging.

Figure 3 shows a simulated PSF obtained by merging the two individually simulated PSFs tailored to each axis observation. This PSF is clearly centrally peaked, contrary to the observations. From the model PSF we calculate a ratio of $R_{PSF} = 5$ between the counts enclosed within a circle of 0.″2 radius centered on the peak of the PSF (identified by a cross in Figure 3), and an adjacent circle of the same radius. A comparison with our longest on-axis observation (17031) gives a consistent ratio (given the large statistical error) when comparing the central circle with the one in a fairly low-surface brightness region at the left (to the east; in blue in Figure 3). Instead, we obtain a ratio of $R_S = 1.6 \pm 0.5$ when comparing the central circle with the one to the south, $\sim 7\sigma$ lower than indicated by the PSF. The shorter on-axis observation (17664) also shows an N-S elongation, albeit with more limited statistics. Within the statistics, the counts from all of the regions shown in the merged images in Figure 3 are consistent in the two separate observations. Using the merged image, we obtain $R_N = 2.1 \pm 0.5$ (5.8σ from the PSF ratio) and $R_S = 1.4 \pm 0.3$ (12σ discrepancy), showing an N-S extension at high statistical significance. Instead, $R_E = 4.2 \pm 1.8$, which is consistent with the PSF. Similar conclusions drawn if instead of directly calculating the statistical errors from the data (using the square root of the counts and propagating them as appropriate), we compare the ratios of the counts from a given region to the nuclear counts from the data with the results of 1000 simulations based on the PSF model normalized to the total number of counts in the extended nuclear region (Figure 4). In these simulations the ratio for the eastern region is also consistent with that expected from a point source.

The above analysis shows that nuclear emission is more complex and extended in the N-S direction than expected from a single point source. This is confirmed by χ^2 tests. We compared via χ^2 data from the N-S and east to west (E-W) with counts from similar regions extracted from the model PSF. We used extraction strips consisting of three adjacent square boxes of 0.″3 side, the central of which includes the higher surface brightness nuclear region (see Figures 2 and 3). Normalizing the PSF either to the counts in central nuclear region, or to the total number of counts in the three bins, we obtain p values of $P \sim 0.02$–0.05 for the E-W direction, suggesting that the count distribution could be marginally consistent with that of a point source. In the N-S direction instead we obtain p values of $P \ll 0.001$ in both cases, showing that the emission is significantly more extended than the PSF.

To get a better definition of the morphology of the N-S Fe Kα structure, we have produced a 1/16 pixel image and processed it with adaptive smoothing, using Gaussian kernels ranging from 0.5 to 10 pixels, 30 iterations, and 5 counts under the kernel. The result is shown in Figure 5. The N-S feature extends for ∼0.″8, corresponding to 65 pc at the assumed distance of 16.9 Mpc.

3. Discussion

High-resolution imaging studies of the *Chandra* ACIS observations in different spectral bands are starting to show the complexity of the inner ($r \sim 100$ pc) circumnuclear regions of CT AGNs. NGC 5643, discussed here, is the first example where ALMA and *Chandra* observations can be used to give a complementary picture of the obscuring torus.

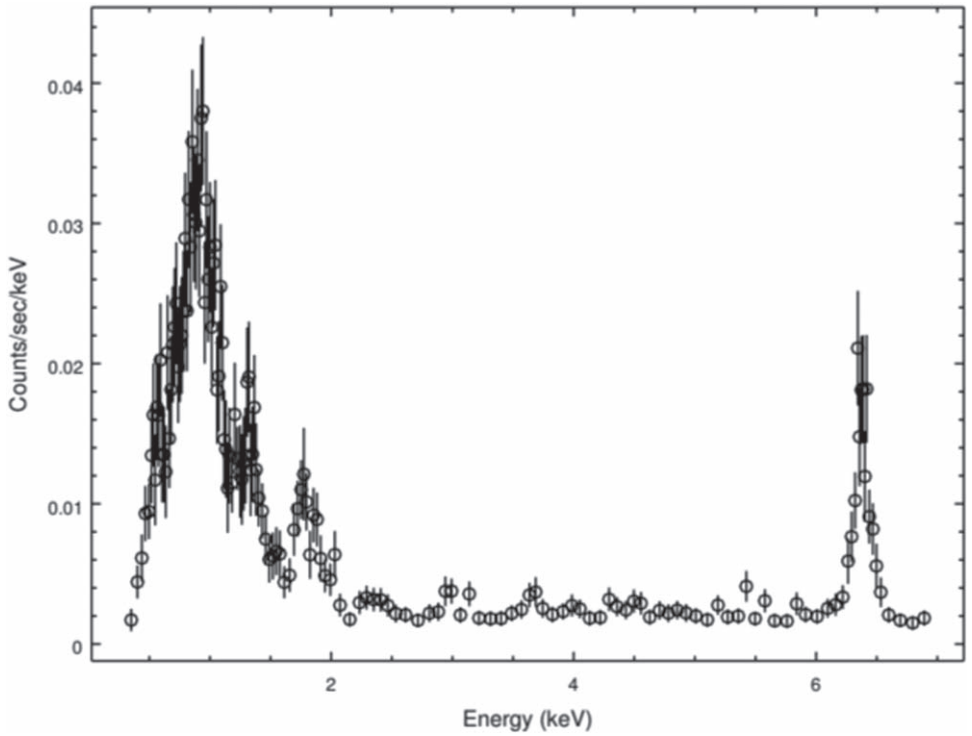

Figure 1. Observed spectral distribution of the nuclear emission of NGC 5643. These counts were extracted from a $\sim 30'' \times 20''$ box enclosing the nucleus and the entire extended emission of the ionization cone.

3.1. Comparison with Other Circumnuclear Regions of CT AGNs Studied with Chandra

In the nearby CT AGN NGC 4945, possibly the best-studied case so far a $\sim 200 \times 100$ pc clumpy flattened distribution perpendicular to the main axis of the ionization cone was detected with *Chandra* in hard continuum ($\sim$3–6 keV), 6.4 keV neutral Fe Kα, and 6.7 keV Fe XXV emission lines (Marinucci et al. 2012, 2017). In the CT AGN ESO 428-G014 (Fabbiano et al. 2018c), two knots of Fe Kα emission are detected with $\sim$30 pc projected separation, embedded in a larger diffuse region of both hard (3–6 keV) continuum and Fe Kα emission, extending out to 1–2 kpc in the direction of the ionization bicone (Fabbiano et al. 2017, 2018a, 2018b). These knots are inclined by $\sim 30^{\circ}$ to the bicone axis, rather than being at $\sim$90 degrees, as in NGC 4945. In NGC 5643, discussed here, the $\sim$65 pc N-S feature we have detected is perpendicular to the ionization cone that extends E-W (Morris et al. 1985; Schmitt et al. 1994; Cresci et al. 2015), as in NGC 4945.

The details of the morphology of these nuclear regions are somewhat energy dependent in all cases. In particular, in NGC 4945 (Marinucci et al. 2017) the equivalent width (EW) of the Fe Kα line is spatially variable (ranging from 0.5 to 3 keV) on scales of tens of parsecs. This EW spatial variability suggests differences in the ionization state and spatial distribution of the optically thick reprocessing clouds, with respect to the central X-ray illuminating source. In ESO 428-G014 (Fabbiano et al. 2018c), we reported an EW of $\sim$1 and $>$2 keV for the nuclear knots.

In NGC 5643, using the regions in Figure 3 and comparing the 6.2–6.6 keV with the 5.0–6.0 keV continuum images, we find the values of the EW consistent with those of NGC 4945 and ESO 428-G014. In particular, EW $= 1.6 \pm 0.5$ keV (north), 1.4 ± 0.3 keV (center), and 2.5 ± 0.8 keV (south). The total Fe Kα EW using counts from a box encompassing the N-S emission is 1.6 ± 0.2. As argued for ESO 428-G014 (Fabbiano et al. 2017), these large EW values exclude that the N-S feature may be due to luminous X-ray binaries. The lack of a corresponding N-S structure in the 3–6 keV continuum reinforces this conclusion and identifies the N-S structure with reflecting Compton-thick circumnuclear clouds.

3.2. The Fe Kα EW of CT AGNs

The EW gives a measurement of the reprocessing of the continuum to generate the Fe Kα line. The Fe Kα EW is typically large in highly obscured CT AGNs. As discussed in Section 3.1, the empirical EW derived from the *Chandra* data by comparing the Fe Kα emission with the $\sim$4–6 keV continuum are all in the $\sim$1–2 keV range and show local variations.

The discovery that much of the Fe Kα emission arises at large distances and has a wide range of the EW (see Fabbiano et al. 2017 and Section 3.1) complicates the use of this EW as a diagnostic tool for AGN evolution. In particular, Boorman et al. (2018) claim an anticorrelation between the Fe Kα EW and continuum luminosity, as measured by the 12 μm luminosity (Asmus et al. 2015). With a 12 μm luminosity of $\sim 10^{43}$ erg s^{-1} (NASA/IPAC Extragalactic Database (NED); Sanders et al. 2003) each of the north, center, and south regions of the N-S feature of NGC 5643 lie above the best-fit correlation in Boorman et al. (2018).

3.3. Imaging the Torus

The idea of AGN obscured by a Compton-thick torus (the standard model; see, e.g., Antonucci 1993) is generally accepted, since it manages to explain several observational characteristics of AGNs. However, it is only recently that we begin to have direct observational evidence of these structures.

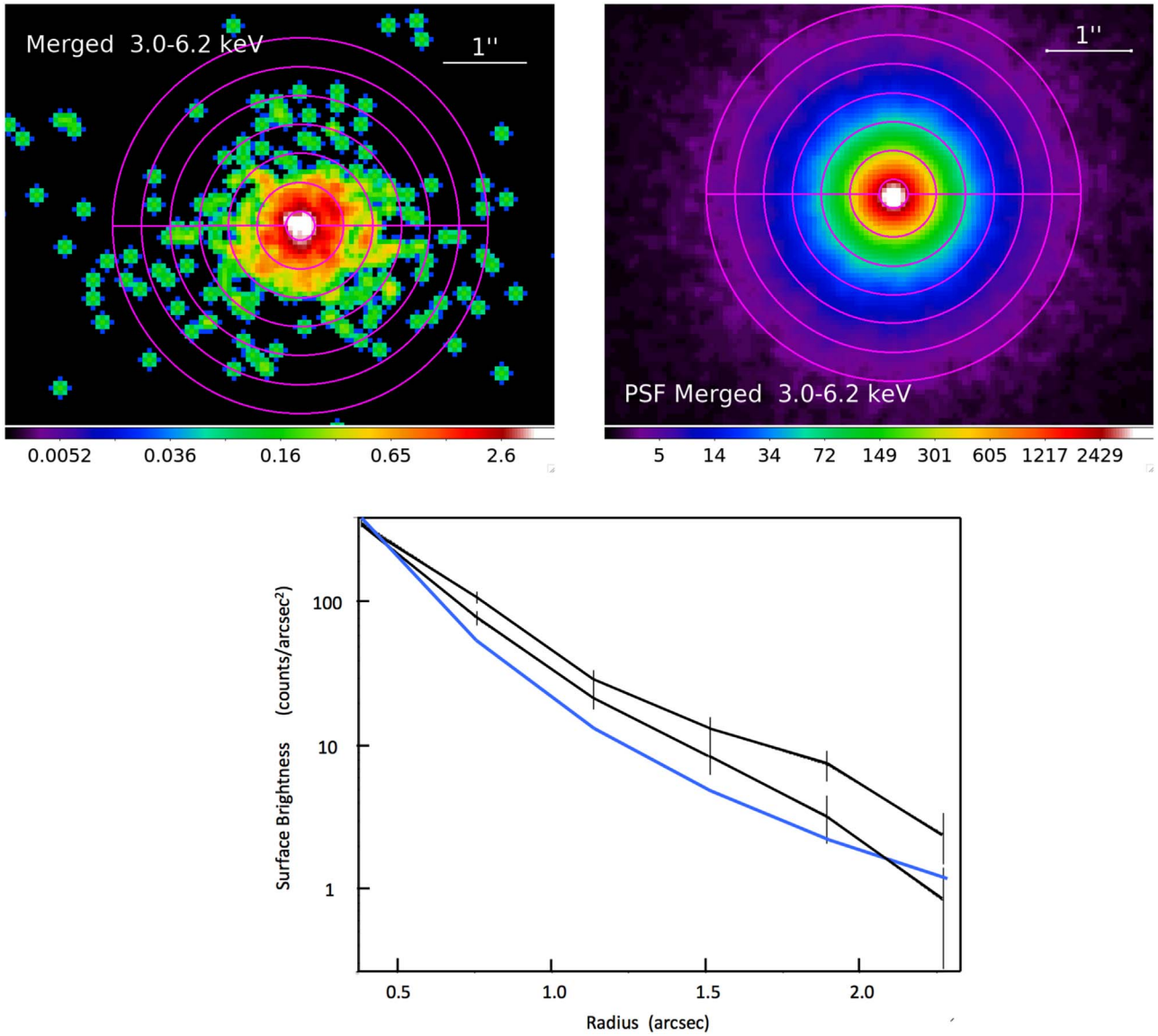

Figure 2. Top left: 1/8 pixel, (3.0–6.2 keV) image of the nuclear region, with a 2 pixel Gaussian smoothing applied for visibility. Top right: the corresponding model PSF. The intensity color scale (in counts/pixel) is given at the bottom of each panel. North is at the top and and east is to the left of each panel. On both images are superimposed extraction regions used to derive the radial profiles shown in the bottom panel. The PSF is in blue and the northern and southern hemispheres from the data are in black.

As the maximum dust sublimation temperature at the nucleus of NGC 4945 (Asmus et al. 2015) implies an inner radius of ~8 pc for the AGN torus, Fabbiano et al. (2018c) argue that the ~10 times larger flattened nuclear distribution of Fe Kα in NGC 4945 may arise from scattering of molecular clouds in a flattened structure in the interstellar medium (ISM) of NGC 4945. Similar large-scale molecular gas is common in other AGN, based on mapping of the H_2 (2.12 μm) emission line of Hicks et al. (2009) who argue that this flattened larger structure is connected with the smaller scale AGN torus based on their co-alignment.

In NGC 5643, the ALMA detection and kinematics of a rotating circumnuclear molecular disk indicate that this disk is unconnected with the general galaxy ISM. The *Chandra* detection of a corresponding N-S structure in the neutral Fe Kα line would argue for both CO and Fe Kα emission originating from the obscuring torus. The ALMA position–velocity diagram shows that, kinematically, the CO disk extends to $\pm$~0.″3, but not to 0.″4 (Alonso-Herrero et al. 2018, their Figure 8). If the entire N-S feature were due to Fe Kα fluorescence of an optically thick scattering disk, this disk would be larger than the ALMA CO disk. However, if we assume that the most luminous clump is coincident with the nucleus, the Fe Kα emission could have the same size as the CO disk if the northernmost clump is not part of this dynamical structure (Figure 5).

The ALMA CO disk has a line of sight of $N_{\rm H} \sim$ few $\times$ 10^{23} cm^{-3} (Alonso-Herrero et al. 2018, Section 4.4). This is ~10 times lower than the minimum Compton-thick $N_{\rm H}$, as seen in the X-ray spectrum (Risaliti et al. 1999). Assuming a similar $N_{\rm H}$ radially from the AGN continuum source then, as in the Hicks et al. (2009) H_2 study, this discrepancy implies a clumpy disk, although as the X-ray nucleus provides only a single point, the requirement is less strong in NGC 5643. In NGC 5643 clear lines of sight ($N_{\rm H} \sim <10^{23}$ cm^{-2}) through the torus are needed to allow the X-ray continuum through to the outer

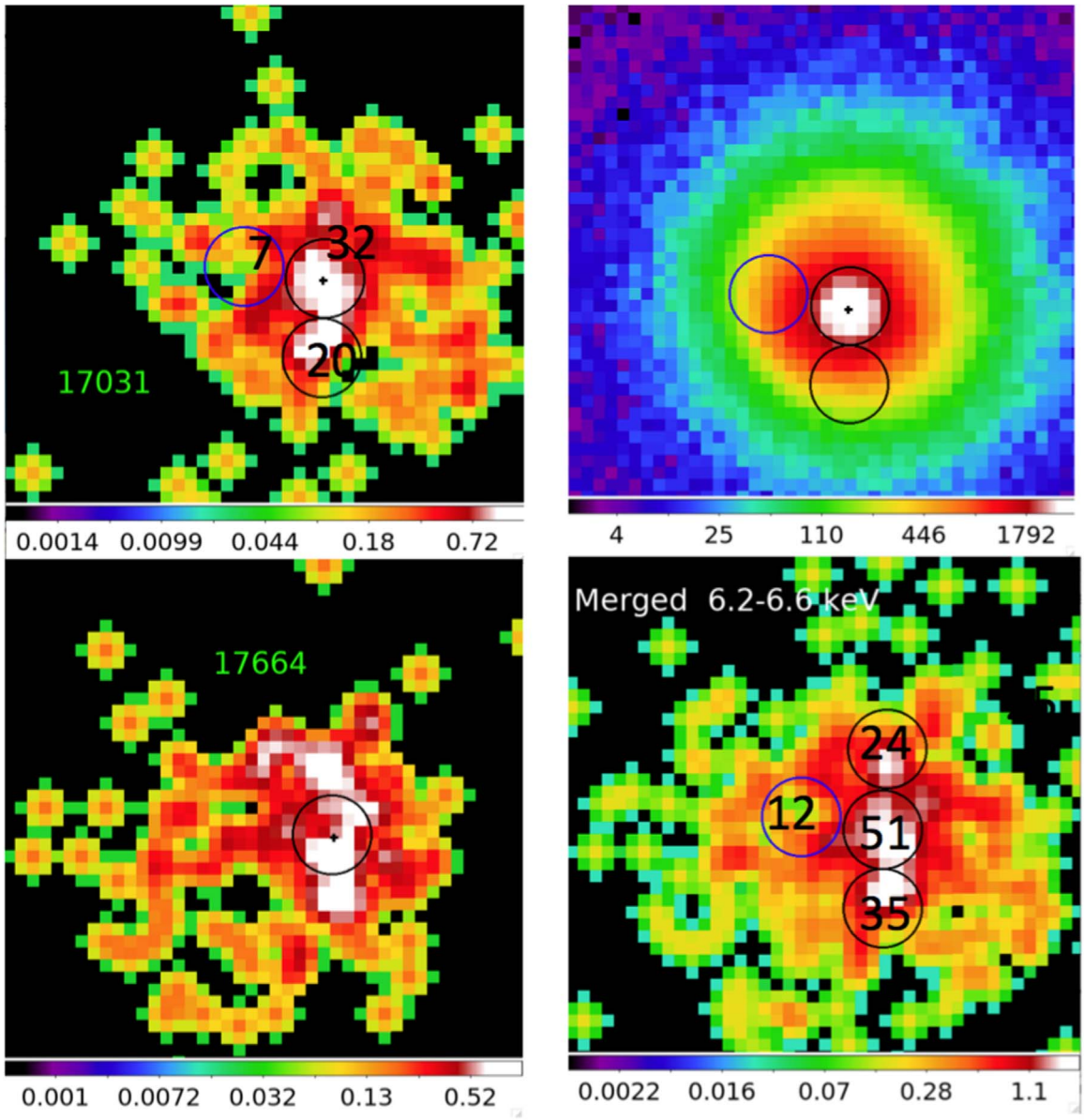

Figure 3. From the bottom panel, clockwise: the merged 6.2–6.6 keV image, the images of the two on-axis observations in the same spectral band, as indicated, and the 6.2–6.6 keV merged PSF. All of the images are binned in 1/8 pixel. The data have been smoothed with a 2 pixel Gaussian for visibility. The intensity color scale (in counts/pixel) is given at the bottom of each panel; these scales are different in each panel. The $0\farcs2$ radius circular extraction areas and counts (see the text) are also plotted. North is at the top and east is to the left of each panel.

molecular clouds where it can create the fluorescent Fe Kα line, i.e., a clumpy torus (Nenkova et al. 2008) with a low-density ($<n_e> \sim <10^3\,\mathrm{cm}^{-2}$) inter-cloud medium, in contrast to some of the torus models (Stalevski et al. 2016). Hicks et al. (2009) also require a clumpy disk.

The ALMA map is slightly asymmetric in CO(2–1) intensity, from $2.0\,\mathrm{Jy\,km\,s^{-1}\,beam^{-1}}$ in the north to $2.4\,\mathrm{Jy\,km\,s^{-1}\,beam^{-1}}$ in the south (Alonso-Herrero et al. 2018, their Figure 5). If we take this as a measure of relative N_H, then the Fe–K emission will be stronger in the south by factor of $e^{-2.0}/e^{-2.4} = 1.5$. If we use the 1/16 image of Figure 5 as a guide, and we exclude the northernmost clump (see above), we find that the ratio between the clump south of the nucleus appears brighter than the one just north of the nucleus. However, the counting statistics are poor, leading to a ratio of 1.7 ± 0.7. Comparison of the northernmost and southernmost clumps show that the southern clump yields slightly more counts, but the two values are compatible within the statistical error.

In NGC 4945 Marinucci et al. (2017) also find also an extended clumpy Fe XXV nuclear feature, with some spatial difference from the neutral Fe Kα structure, which could highlight regions of prevalent shock excitation. In NGC 5643 the 6.6–6.9 keV emission shows a single peak, consistent with the continuum peak.

4. Summary and Conclusions

Our conclusions are summarized as follows.

1. Imaging the deep on-axis *Chandra* ACIS observations of the CT AGN NGC 5643 in the 6.2–6.6 keV Fe Kα line, we have found a significant elongated feature in the nuclear region. This feature is clumpy and extends for

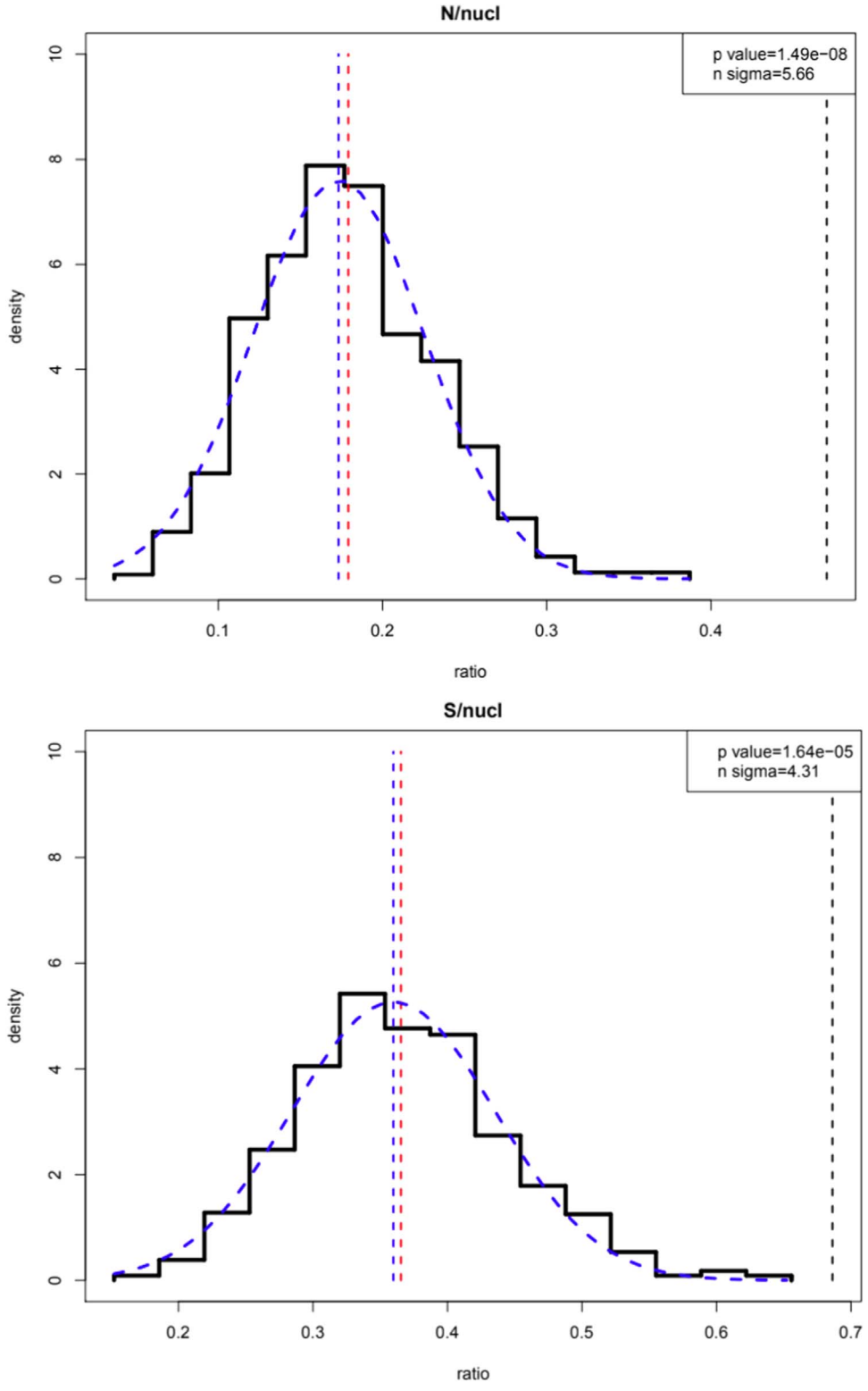

Figure 4. Probability density distributions of the simulated ratios from 1000 instances of a model PSF normalized to the total counts in the 6.2–6.6 keV extended nuclear region (solid line). Top: ratio of the region north of the nucleus in Figure 3 relative to the nucleus. Bottom, same for the region south of the nucleus in Figure 3. The Gaussian fits to the distributions are represented by the blue dashed lines, with a mean indicated by the vertical dashed blue line. The ratio in the PSF model is indicated by the vertical red dashed line, and the observed ratio in the region is indicated by a vertical dashed black line. The probability of observing such ratios given the fitted Gaussian distribution and the equivalent sigmas are indicated in the box.

∼65 pc N-S and no corresponding feature is seen in the 3.0–6.0 keV continuum.

2. We find EWs of 1.6 ± 0.5 keV (north), 1.4 ± 0.3 keV (center), and 2.5 ± 0.8 keV (south). The total Fe Kα EW using counts from a box encompassing the N-S emission is 1.6 ± 0.2
3. The Fe Kα feature is spatially consistent with the N-S elongation found in the CO(2–1) high-resolution imaging

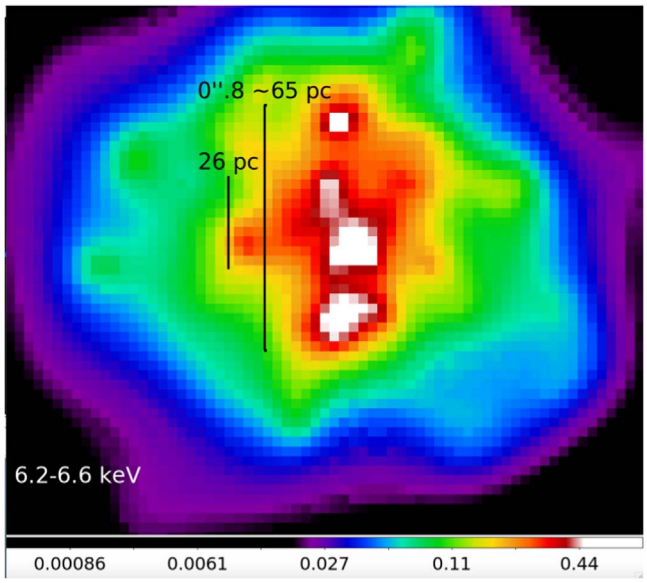

Figure 5. Left: adaptively smoothed image of the 6.2–6.6 keV nuclear emission with 1/16 pixels (see the text). We show also the size of the ALMA disk (26 pc; Alonso-Herrero et al. 2018). The intensity color scale (in counts/pixel) is given at the bottom. North is at the top and east is to the left.

with ALMA (Alonso-Herrero et al. 2018), but more extended than the rotating molecular disk of diameter 26 pc indicated by the kinematics of the CO(2–1) line.

4. The *Chandra* detection of a corresponding N-S structure in the neutral Fe Kα line would argue for both CO and Fe Kα emission originating from the obscuring torus.
5. Both the clumpiness of the Fe Kα map and the relatively low $N_{\rm H} \sim$ few $\times\ 10^{23}\,{\rm cm}^{-3}$ derived from the ALMA data (Alonso-Herrero et al. 2018; Section 4.4) suggest a clumpy obscuring circumnuclear disk.

In conclusion, both high-resolution *Chandra* X-ray data and ALMA observations in the submillimeter range are beginning to provide direct pictures of the circumnuclear regions of CT AGNs. These observations are complementary in that the hard X-ray and Fe Kα emission are due to AGN photons scattered by circumnuclear Compton-thick clouds, while the molecular clouds themselves are directly revealed via their CO emission with ALMA. NGC 5643, discussed here, is the first instance of a CT AGN with both Fe Kα and CO (2–1) observations at scales of $<$100 pc where both windows suggest an N-S Compton-thick feature that could be connected with the torus of the standard AGN model.

A full study of the X-ray emission of NGC 5643, including spectral modeling, will be presented in a forthcoming paper.

Larger scale *Chandra* imaging in the hard X-ray continuum and Fe Kα line has also shown that these emissions are not just confined to the immediate circumnuclear region. They can arise at radii as large as a few kiloparsecs. These features suggest interaction with dense molecular clouds in the host galaxy disk (Fabbiano et al. 2017, 2018a, 2018b), opening the way for future joint *Chandra*—ALMA studies. These exploratory deep *Chandra* observations argue the need for a large-area, high-resolution future X-ray observatory, such as *Lynx*, to pursue observational studies of AGN—galaxy interaction in detail in a large number of AGNs.

We retrieved data from the NASA-IPAC Extragalactic Database (NED) and the Chandra Data Archive. For the data analysis, we used the CIAO toolbox and DS9, developed by the Chandra X-ray Center (CXC). This work was partially supported by the Chandra Guest Observer program grant GO5-16090X (PI: Fabbiano) and NASA contract NAS8-03060 (CXC).

ORCID iDs

G. Fabbiano https://orcid.org/0000-0002-3554-3318
A. Paggi https://orcid.org/0000-0002-5646-2410
M. Elvis https://orcid.org/0000-0001-5060-1398

References

Alonso-Herrero, A., Pereira-Santaella, M., Garcia-Burillo, S., et al. 2018, ApJ, 859, 144
Annuar, A., Gandhi, P., Alexander, D. M., et al. 2015, ApJ, 815, 36
Antonucci, R. 1993, ARA&A, 31, 473
Asmus, D., Gandhi, P., Höning, S. F., Smette, A., & Duschl, W. J. 2015, MNRAS, 454, 766
Boorman, P. G., Gandhi, P., Baloković, M., et al. 2018, MNRAS, 477, 3775
Cresci, G., Marconi, A., Zibetti, S., et al. 2015, A&A, 582, 63
Fabbiano, G., Elvis, M., Paggi, A., et al. 2017, ApJL, 842L, 4
Fabbiano, G., Paggi, A., Karovska, M., et al. 2018a, ApJ, 855, 131
Fabbiano, G., Paggi, A., Karovska, M., et al. 2018b, ApJ, 865, 83
Fabbiano, G., Siemiginowska, A., Paggi, A., et al. 2018c, ApJ, in press (arXiv:1811.06436)
Fruscione, A., McDowell, J. C., Allen, G. E., et al. 2006, Proc. SPIE, 6270, 62701V
Guainazzi, M., Rodriguez-Pascual, P., Fabian, A. C., Iwasawa, K., & Matt, G. 2004, MNRAS, 355, 297
Hicks, E. K. S., Davies, R. I., Malkan, M. A., et al. 2009, ApJ, 696, 448
Levenson, N. A., Heckman, T. M., Krolik, J. H., Weaver, K. A., & Życki, P. T. 2006, ApJ, 648, 111
Marinucci, A., Bianchi, S., Fabbiano, G., et al. 2017, MNRAS, 470, 4039
Marinucci, A., Risaliti, G., Wang, J., et al. 2012, MNRAS, 423, L6
Matt, G., Bianchi, S., Marinucci, A., et al. 2013, A&A, 556, 91
Morris, S. L., Ward, M. J., Whittle, M., Wilson, A. S., & Taylor, K. 1985, MNRAS, 216, 193
Nenkova, M., Sirocky, M. M., Nikutta, R., Ivezic, Z., & Elitzur, M. 2008, ApJ, 685, 160
Risaliti, G., Maiolino, R., & Salvati, M. 1999, ApJ, 522, 157
Sanders, D. B., Mazzarella, J. M., Kim, D.-C., Surace, J. A., & Soifer, B. T. 2003, AJ, 126, 1607
Schmitt, H. R., Storchi-Bergmann, T., & Baldwin, J. A. 1994, ApJ, 423, 237
Stalevski, M., Ricci, C., Ueda, Y., et al. 2016, MNRAS, 458, 2288